



HAL
open science

Solar wind interaction with comet 67P: Impacts of corotating interaction regions

J T Edberg, I I Eriksson, E Odelstad, E Vigren, D J Andrews, F J Johansson, J L Burch, C M Carr, E Cupido, K. H. Glassmeier, et al.

► **To cite this version:**

J T Edberg, I I Eriksson, E Odelstad, E Vigren, D J Andrews, et al.. Solar wind interaction with comet 67P: Impacts of corotating interaction regions. *Journal of Geophysical Research Space Physics*, 2016, 121 (2), pp.949 - 965. 10.1002/2015JA022147 . insu-01316542

HAL Id: insu-01316542

<https://insu.hal.science/insu-01316542>

Submitted on 29 Nov 2016

HAL is a multi-disciplinary open access archive for the deposit and dissemination of scientific research documents, whether they are published or not. The documents may come from teaching and research institutions in France or abroad, or from public or private research centers.

L'archive ouverte pluridisciplinaire **HAL**, est destinée au dépôt et à la diffusion de documents scientifiques de niveau recherche, publiés ou non, émanant des établissements d'enseignement et de recherche français ou étrangers, des laboratoires publics ou privés.

1 Solar wind interaction with comet 67P: impacts of
2 corotating interaction regions

N. J. T. Edberg,¹ A. I. Eriksson,¹ E. Odelstad,^{1,2} E. Vigren,¹ D. J. Andrews,¹
F. Johansson,¹ J. L. Burch,³ C. M. Carr,⁴ E. Cupido,⁴ K.-H. Glassmeier,⁵ R.
Goldstein,³ J. S. Halekas,⁶ P. Henri,⁷ C. Koenders,⁵ K. Mandt,³ P. Mokashi,³
Z. Nemeth,⁸ H. Nilsson,⁹ R. Ramstad,⁹ I. Richter,⁵ G. Stenberg Wieser⁹

3 **Abstract.** We present observations from the Rosetta Plasma Consortium
4 of the effects of stormy solar wind on comet 67P/Churyumov-Gerasimenko.
5 Four corotating interaction regions (CIRs), where the first event has possi-
6 bly merged with a CME, are traced from Earth via Mars (using Mars Ex-
7 press and MAVEN) and to comet 67P from October to December 2014. When
8 the comet is 3.1-2.7 AU from the Sun and the neutral outgassing rate $\sim 10^{25}$ —

N. J. T. Edberg, A. I. Eriksson, E. Odelstad, E. Vigren, D. J. Andrews, F. Johansson, Swedish
Institute of Space Physics, Uppsala, Box 537, SE-75121, Sweden

J. L. Burch, R. Goldstein, K. Mandt, P. Mokashi, Southwest Research Institute, 6220 Culebra
Rd., San Antonio, TX 78238, USA

C. Carr, E. Cupido, Imperial College London, Exhibition Road, London SW7 2AZ, United
Kingdom

K.-H. Glassmeier, C. Koenders, I. Richter, TU - Braunschweig, Institute for Geophysics and
extraterrestrial Physics, Mendelssohnstr. 3

J. Halekas, University of Iowa, Iowa City, Iowa, USA

P. Henri, Laboratoire de Physique et Chimie de l'Environnement et de l'Espace, Orleans Cedex
2, France

Z. Nemeth, Wigner Research Institute, Budapest, HUngary

H. Nilsson, G. Stenberg Wieser, R. Ramstad, Swedish Institute of Space Physics, Box 812, 981
28 Kiruna, Sweden

¹Swedish Institute of Space Physics,

9 10^{26} s^{-1} the CIRs significantly influence the cometary plasma environment
10 at altitudes down to 10-30 km. The ionospheric low-energy ($\sim 5 \text{ eV}$) plasma

Uppsala, Sweden (ne@irfu.se)

²Department of Physics and Astronomy,
Uppsala University, Uppsala, Sweden

³Southwest Research Institute, San
Antonio, USA

⁴Space and Atmospheric Physics Group,
Imperial College London, UK

⁵TU - Braunschweig, Institute for
Geophysics and Extraterrestrial Physics,
Braunschweig, Germany

⁶Department of Physics and Astronomy,
University of Iowa, Iowa City, IA, USA

⁷Laboratoire de Physique et Chimie de
l'Environnement et de l'Espace, Orleans,
France

⁸Wigner Research Center for Physics,
Budapest, Hungary

⁹Swedish Institute of Space Physics,
Kiruna, Sweden

11 density increases significantly in all events, by a factor > 2 in events 1-2
12 but less in events 3-4. The spacecraft potential drops below -20V upon im-
13 pact when the flux of electrons increases. The increased density is likely caused
14 by compression of the plasma environment, increased particle impact ion-
15 isation, and possibly charge exchange processes and acceleration of mass loaded
16 plasma back to the comet ionosphere. During all events, the fluxes of suprather-
17 mal (~ 10 -100 eV) electrons increase significantly, suggesting that the heat-
18 ing mechanism of these electrons is coupled to the solar wind energy input.
19 At impact the magnetic field strength in the coma increases by a factor of
20 2-5 as more interplanetary magnetic field piles up around of the comet. Dur-
21 ing two CIR impact events, we observe possible plasma boundaries forming,
22 or moving past Rosetta, as the strong solar wind compresses the cometary
23 plasma environment. We also discuss the possibility of seeing some signa-
24 tures of the ionospheric response to tail disconnection events.

1. Introduction

25 The interaction of the solar wind with a cometary plasma environment has previously
26 only been studied in situ during satellite flybys. With Rosetta in orbit around comet
27 67P/Churyumov-Gerasimenko (hereafter 67P), it is now possible to study the interaction
28 over longer periods of time, and especially to study how the cometary magnetosphere
29 responds to variations in the solar wind.

30 Rosetta arrived at comet 67P on 6 August 2014, to begin conducting continuous mea-
31 surements of the near-nucleus (< 100 km) plasma environment as well as of the neutral
32 gas and dust. During the autumn of 2014 Rosetta gradually and slowly approached the
33 comet, moving with a velocity on the order of 1 m/s, and reaching a minimum altitude
34 of about 10 km during October. The comet lowered its heliocentric distance from 3.1 to
35 2.7 AU, in the interval from 1 Oct 2014 - 1 Jan 2015.

36 At the arrival of Rosetta in August 2014, the comet was relatively inactive and had
37 just begun to form an induced magnetosphere in the solar wind [Nilsson *et al.*, 2015].
38 The neutral outgassing rate from the comet was measured to be $\sim 10^{25}$ s $^{-1}$ [Gulkis *et al.*,
39 2015]. As the emitted neutral gas becomes ionised, predominantly through photoioniza-
40 tion, particle impacts and/or charge exchange processes [Cravens *et al.*, 1987; Burch *et al.*,
41 2015; Vigren *et al.*, 2015] an ionosphere, which initially expands radially outward, forms
42 around the comet nucleus. As the comet approaches the sun, the ionosphere grows and
43 becomes denser, and the induced magnetosphere concurrently expands. The density of
44 the ionospheric plasma close to the nucleus decreases with distance as $1/R$ [Edberg *et al.*,

45 2015], in agreement with theory simplified by the neglect of field influence and chemical
46 loss [*Vigren et al.*, 2015].

47 Pickup ions of cometary origin have been observed since arrival and have evolved with
48 time to become more energetic closer to the Sun [*Goldstein et al.*, 2015; *Nilsson et al.*,
49 2015]. The outgassing of neutrals was found to be quite inhomogeneous and most of the
50 gas was observed over the neck region of the comet [*Hässig et al.*, 2015]. *Edberg et al.*
51 [2015] mapped the ionospheric plasma and found it to be distributed similarly as the
52 neutrals, indicating that plasma from local ionisation of neutrals (in the region between
53 the nucleus and Rosetta) dominated the cold plasma environment. This also implies
54 that the ionospheric structure is modulated by the comet spin period. Furthermore,
55 67P was found to have a plasma environment that is full of small scale density and
56 magnetic field variations and where instabilities and waves are common [*Richter et al.*,
57 2015], complicating the interaction with the solar wind. *Volwerk et al.* [2016] reported
58 on observations of mirror-mode waves that were generated following a compression of
59 the plasma environment due to increased solar wind dynamic pressure. A population
60 of suprathermal electrons ($\sim 10 - 100$ eV) has been observed continuously after arrival,
61 although with significant variations in both energy and flux over time [*Clark et al.*, 2015].

62 Comet 67P is a relatively weakly outgassing comet and no bow shock, diamagnetic
63 cavity or ionopause, for instance, was observed in the interval covered in this paper, i.e.
64 until 1 Jan 2015. Some piling-up of the interplanetary magnetic field (IMF) was occurring
65 but no constant pile-up boundary was observed, which is in agreement with predictions
66 from simulations [*Koenders et al.*, 2013; *Rubin et al.*, 2014]. The ion instruments on
67 Rosetta were able to measure the solar wind more or less continuously since arrival (until

68 the end of March of 2015 when the coma had grown), although significant deflection of
69 the solar wind, by more than 45 degrees, was observed [*Nilsson et al.*, 2015; *Broiles et al.*,
70 2015].

71 In this paper we will specifically study the response of the cometary plasma environment
72 to stormy space weather, when impacts of corotating interaction regions (CIR) occur. The
73 purpose is to identify the main effects these solar wind pressures pulses have on the comet
74 ionosphere.

75 CIRs form when slow solar wind is caught up by faster solar wind and an interaction
76 region forms in between the two flows, typically characterised by an increased magnetic
77 field strength, plasma density and pressure. Across the CIR, the magnetic field polarity
78 often reverses. The slow and fast solar winds emanate from specific regions on the Sun,
79 which can be emitting plasma similarly during several solar rotations (one solar rotation
80 being approximately 27 days) such that an interaction region is continuously formed.
81 As the Sun rotates, this interaction region will sweep across the heliosphere while also
82 expanding radially outward, until it eventually impacts on any planet, moon or comet in
83 its way, where it most likely will cause a significant disturbance to the plasma environment.
84 At Mars and Venus, CIR impacts have been shown to increase the ionospheric escape
85 rates[e.g *Dubinin et al.*, 2008; *Edberg et al.*, 2009, 2010, 2011]. CIRs are typically less
86 impulsive than coronal mass ejections (CME), but are instead a more common and regular
87 phenomena in interplanetary space since they emanate from coronal holes that are more
88 stable in time. CMEs propagate mainly radially outward (with some angular spread), but
89 can often merge with any slower CIR ahead of it.

90 CME impacts on comets have been observed to lead to so called tail disconnection
91 events, when oppositely directed magnetic fields in the tail of the comet reconnect with
92 each other [*Vourlidas et al.*, 2007]. A plasmoid then forms which disconnects from the
93 comet [*Niedner and Brandt*, 1978]. Similar events could also occur during CIR impact
94 events. Since Rosetta is always orbiting relatively close to the nucleus any tail discon-
95 nection event happening far down the tail will, most likely, not be directly observed by
96 Rosetta, but the effects of it closer to the nucleus might still be observed.

97 We will present measurements from the plasma environment around comet 67P during
98 4 separate CIR impacts to study how the comet magnetosphere is affected during such
99 events. We have limited our study to 3 months (1 October 2014 - 1 January 2015) when
100 the comet was at heliocentric distances of 3.1-2.7 AU and relatively inactive (outgassing
101 $\sim 10^{25} - 10^{26} \text{ s}^{-1}$). The study is naturally limited in space and time to where Rosetta was
102 located in this interval, i.e. in orbit at an altitude of 10-30 km and close to the terminator
103 plane. The paper is organised as follows: first we introduce the instruments used in this
104 paper, followed by a section describing CIR propagation from Earth, via Mars and finally
105 to 67P. We then present measurements from Rosetta at 67P during the CIR impacts, and
106 finish with a discussion and summary.

2. Instruments

107 The Rosetta spacecraft carries five instruments for measuring plasma properties as
108 well as magnetic and electric fields around the comet. These form the Rosetta Plasma
109 Consortium (RPC) [*Carr et al.*, 2007]. In this paper we will present a combined data set
110 from all instruments. Each individual instrument is briefly described below.

111 The Langmuir probe instrument (LAP) [*Eriksson et al.*, 2007] consists of two spherical
112 Langmuir probes (LAP1 and LAP2), mounted on booms, 2.2 m and 1.6 m long, respec-
113 tively, from hinge to probe. Here we will mainly use data from LAP1 when in ‘sweep’
114 mode, to obtain the ion and electron density as well as the spacecraft potential at a ca-
115 dence of normally 96 s or 160 s. From the Langmuir probe sweeps both the electron and
116 ion density can be obtained. However, when the spacecraft potential is very negative
117 (which it often is during the interval studied in this paper due to high fluxes of ~ 5 eV
118 electrons) the electrons are to a large extent accelerated away from the probe and the
119 electron density obtained by the probe sweeps is underestimated. Regarding the ions, the
120 instrument sweep range has not always been set to sufficiently low negative values to fully
121 sample the undisturbed ion current and the ion density estimate is then more uncertain.
122 During intervals of very negative spacecraft potential the ions are fortunately more eas-
123 ily attracted by the probe. Still, this sweep range limitation leads us to use the sweep
124 derived electron density estimate during intervals when the sweep is limited to above -5
125 V, while otherwise we use the ion density estimate. Furthermore, we are also able to use
126 the measured spacecraft potential obtained from the sweeps as a proxy for the electron
127 density. This density estimate is also dependent on the electron temperature, which most
128 of the time is about 5 eV [*Odelstad et al.*, 2015]. In addition to the sweep mode, LAP
129 can also be run with a fixed bias-potential, where the probe attracts an ion (or electron)
130 current when the probe potential is set to a positive (negative) voltage. When possible,
131 the LAP-derived densities are crosschecked with data from the mutual impedance probe
132 (MIP), described next.

133 The MIP instrument [*Trotignon et al.*, 2007] consists of two receiving and two transmit-
134 ting electrodes, mounted on the same boom as LAP1. MIP is able to retrieve the electron
135 density from the position of the electron plasma frequency in the mutual impedance spec-
136 tra. MIP can operate in two different ways: in short Debye length (SDL) mode by using
137 one or two of its own transmitters situated at 40 and 60 cm from the receivers, or in
138 long Debye length (LDL) mode when using the LAP2 probe as transmitter, at a dis-
139 tance of about 4 m from the MIP receivers. The SDL and LDL modes cannot be run
140 simultaneously.

141 On the one hand, when the spacecraft potential becomes more negative than the LAP
142 sweep range, it is not possible to obtain the electron density from the LAP sweeps. On the
143 other hand, MIP can retrieve plasma parameters only when (i) the ratio of the transmitter-
144 receiver baseline length to the Debye length is large enough, and (ii) when the electron
145 plasma frequency is in the operated MIP frequency range, which is limited to 7-168 kHz
146 in the LDL mode. This explains why, in the early stage of the low comet activity with
147 little cooling of electrons, there is a gap (about $350 - 1000 \text{ cm}^{-3}$) between the density
148 ranges covered by the LDL and SDL modes. Comparing the observations from the MIP
149 and LAP experiments allows us to be more confident about the plasma density estimates.

150 The magnetometer (MAG) [*Glassmeier et al.*, 2007] uses two triaxial fluxgate sensors
151 mounted on the same boom as LAP2, and provides vector measurements of the magnetic
152 field. Here we use 1 min averages from the outboard sensor, which is located 15 cm further
153 out on the boom (and therefore less affected by the spacecraft generated fields). The
154 magnetic field is shown in the comet centered solar equatorial coordinate system (CSEQ).
155 In this system the x-axis points from the comet to the Sun, the z-axis is the component of

156 the Sun's north pole orthogonal to the x-axis, and the y-axis completes the right-handed
157 reference frame.

158 The ion and electron sensor (IES) [Burch *et al.*, 2007] consists of two electrostatic
159 plasma analyzers, one for ions and one for electrons. Both analyzers measure in the
160 energy/charge range 1 eV/q - 18 keV/q in 128 steps with a resolution of 8% and a field of
161 view of $90^\circ \times 360^\circ$. The angular resolution is $5^\circ \times 22.5^\circ$ for electrons and $5^\circ \times 45^\circ$ for ions.
162 Of particular interest here, the anodes facing the solar wind flow are further segmented
163 into $5^\circ \times 5^\circ$ sectors. A full 3D scan of the instrument typically takes 256 s.

164 The ion composition analyzer (ICA) [Nilsson *et al.*, 2007] also measures the ion distri-
165 bution, in the energy range 10 eV - 40 keV with a field of view of $90^\circ \times 360^\circ$, and can
166 in addition resolve masses with a resolution high enough to separate e.g. protons, helium
167 and water group ions. The angular resolution is $5^\circ \times 22.5^\circ$ and a full 3D scan takes 192
168 s. For technical reasons, ICA was only on intermittently during the first months after
169 arrival and began more continuous operations in 2015. This unfortunately leaves many
170 data gaps for the events presented in this paper.

171 Furthermore, in order to monitor the solar wind density and velocity for tracking solar
172 wind structures propagating toward Rosetta and comet 67P, we make use of solar wind
173 measurements from the ACE spacecraft, at Earth's first Lagrange point, as well as mea-
174 surements from the particle instruments on Mars Express and the Mars Atmosphere and
175 Volatile Evolution mission (MAVEN) in orbit around Mars. Mars Express and MAVEN
176 both spend parts of their orbits in the undisturbed solar wind and can then measure its
177 density and velocity [Halekas *et al.*, 2013; Ramstad *et al.*, 2015]. Mars Express carries the

178 analyzer of space plasmas and energetic ions (ASPERA-3) [*Barabash et al.*, 2006], while
179 MAVEN carries the solar wind ion analyzer (SWIA) [*Halekas et al.*, 2013].

3. Observations

3.1. CIR observations at Earth, Mars and 67P

180 Figure 1 shows the positions of Earth, Mars and comet 67P from 1 October 2014 to 1
181 January 2015. Earth was ahead of 67P in heliospheric longitude by more than 45° during
182 the entire interval, while Mars was more or less in the same longitude sector, and in that
183 respect quite suitable for monitoring the solar wind upstream of the comet. However,
184 since the radial distance between Mars and comet 67P was at least 1.2 AU during the
185 interval studied in this paper, any solar wind structure passing by Mars might evolve
186 significantly in both density and velocity profile before reaching 67P.

187 Between 1 October 2014 and 1 January 2015 four events of solar wind pressure pulses
188 (high solar wind velocity, plasma fluxes, pressure, magnetic field) were observed in satellite
189 data from each body. These four events are shown in Figure 2 and are indicated by red
190 vertical lines in ACE data (Figure 2a-b), in Mars Express and MAVEN data (Figure 2c-d)
191 and in Rosetta data (Figure 2e). The start of each event is identified by eye from the
192 data, primarily from the when the solar wind velocity starts to increase. At 67P, the
193 solar wind proton energy (which can be translated to velocity) is indicated by the bright
194 yellow line at about 1 keV, in Figure 2e. Note that the solar wind density is not easily
195 derived from Rosetta data as the S/C environment is dominated by plasma of cometary
196 origin [*Edberg et al.*, 2015]. In Figure 2e we also show modeled solar wind velocity from
197 the Michigan Solar Wind Model (mSWIM) model [*Zieger and Hansen*, 2008]. This model
198 uses an 1.5-D MHD code to propagate solar wind parameters from Earth out to Rosetta.

199 Although the alignment between the Earth and 67P is not ideal for this comparison, there
200 is a general good agreement between the model results and the IES data on how the solar
201 wind velocity varies in this interval.

202 The CIR structures impact on comet 67P on 22 Oct, 7 Nov, 27 Nov and 22 Dec
203 2014. Each event can be fairly easily traced back toward the Sun using the Mars Ex-
204 press/MAVEN and ACE solar wind monitoring data. The fact that it is possible to track
205 them to Earth and Mars despite the large longitudinal separation ($\sim 70^\circ$ between Earth
206 and 67P), indicates that these structures (at least the last three events) are CIRs. The
207 first event is in fact probably a CIR that has merged with a coronal mass ejection (CME),
208 observed to have been ejected from the Sun on 14 Oct 2014. In any case, in terms of veloc-
209 ity and density enhancement there is not much difference during the merged CME/CIR
210 event and the three CIRs. For simplicity, we will therefore refer to the four cases as CIRs.

211 The four CIRs pass by Mars and Earth approximately when expected, as determined
212 from when they are observed to pass by 67P. If assuming that these structures are CIRs,
213 they should propagate radially outward with the solar wind speed and sweep interplane-
214 tary space with the Sun's rotation speed. To estimate the delay time from one location
215 in interplanetary space to another, one has to take into account both the radial and the
216 longitudinal time delay.

217 The radial propagation time from Earth to 67P at 3.1 AU is about 9 days, and to 67P
218 when at 2.7 AU about 7.3 days, if assuming a radial solar wind velocity of 400 kms^{-1} .
219 The longitudinal time difference between Earth and 67P in early October (the time it
220 takes the Sun to turn 70°) is about 5.3 days assuming a solar rotation period of 27 days.
221 Any solar wind structure passing by Earth in October should arrive at the comet roughly

222 $9 - 5.3 = 3.7$ days later. Similarly, a solar wind structure passing by Earth in late
223 December (when Earth and 67P are separated by almost 150° , i.e. 11.2 days) should have
224 arrived at the comet about $7.3 - 11.2 = 3.9$ days earlier. This matches up reasonably well
225 with the velocity structures indicated by the red lines in the time series of solar wind data
226 in Figure 2a and Figure 2e. The actual time delay between the events observed at Earth
227 and at 67P are 3.1 days, 1.1 days, 2.0 days and 3.0 days, respectively.

228 If comparing Mars and 67P, a solar wind structure travelling at 400 kms^{-1} that passes by
229 Mars in October should arrive roughly 7 days later at 67P, when almost radially aligned.
230 In late December, when the longitudinal separation between Mars and 67P has increased
231 to about 40° , a CIR would be seen about 3 days earlier at 67P. This also seems to be
232 the case from the comparison of arrival times of velocity peaks in Figure 2c and Figure
233 2e. Finally, comparing ACE and Mars one notes that during the entire autumn there is
234 a $\sim 90^\circ$ longitudinal separation between Earth and Mars, meaning that a CIR would be
235 observed first at Mars and then about 4 days later at ACE.

236 The individual CIRs are not exactly separated in time by one solar rotation, suggesting
237 that the events are really different CIRs, which originate from different locations on the
238 Sun or that the source region on the Sun has changed. Also, when reaching the heliocentric
239 distance of 67P the original events seen at ACE have possibly had time to evolve and merge
240 with other solar wind structures. If looking again at the time series of ACE data, Figure
241 2a, we note e.g. that the second CIR observed in the ACE data, on 5 November, is
242 surrounded by three additional velocity peaks with successively increasing velocity from
243 1 - 16 November. These four peaks only show up as one single structure at Mars on 4
244 November, indicating that these structures have either merged, the source region on the

245 Sun has changed or, possibly, that some of the smaller peaks seen by ACE were not CIRs
246 but rather smaller CMEs.

247 In summary, tracking CIRs from Earth out to 67P at 3 AU and predicting their arrival
248 times is possible, although somewhat uncertain and their definition to some extent sub-
249 jective. Nevertheless, and most importantly for this study, in Rosetta RPC-IES data four
250 clear events are observed in the ion spectrogram and manifested as sudden increases in
251 the solar wind flux and energy, which are interpreted as CIR impacts.

252 During this interval Rosetta was in bound orbit around the comet at a distance mainly
253 between 10 km and 30 km from the nucleus centre of mass, and mainly in the terminator
254 plane. The trajectory of Rosetta around the times of impacts is shown in Figure 3 in the
255 cometocentric solar orbital (CSO) reference frame. In the CSO frame the x-axis is directed
256 toward the sun, the z-axis is parallel to the comet's orbital angular momentum vector and
257 the y-axis completes the right-handed system. The intervals covered correspond to the
258 time series to be shown in the following four figures (Figures 4-8). The times of impact
259 are indicated by red circles. Next we will present RPC measurements from the cometary
260 plasma environment during the impacts of these CIRs.

3.2. Event 1: 22 Oct 2014

261 Figure 4 shows a time series of combined RPC data around the time of impact of the
262 first CIR to be studied in detail. Rosetta was at this time in orbit at 10 km from the comet
263 nucleus centre of mass and initially moving to northern latitudes. On 22 Oct 2014 at 16:30
264 UT, indicated by the red vertical line, a significant disturbance appeared in the plasma
265 environment of comet 67P. In the RPC measurements essentially all parameters shown in
266 Figure 4a-f show significant changes: the LAP ion current (negative voltage side of the

267 sweeps in panel a) suddenly increases by about -20 nA, the MAG magnetic field strength
268 increased from about 5 nT to on average 30 nT in combination with a change of the
269 magnetic field direction, the IES suprathermal (~ 10 -100 eV) electron counts increased by
270 roughly one order of magnitude together with a general increase in energy of the electrons.
271 The IES-measured solar wind ion energy increased, and the ICA solar wind fluxes (red
272 dots in Figure 4g) increased gradually by almost two orders of magnitude. The count rate
273 of accelerated water ions also suddenly increased. This is identified as the impact of the
274 CIR.

275 Immediately after impact the spacecraft potential became more negative than the LAP
276 instrument sweep range. The LAP sweep probe potential did not go to sufficiently high
277 positive bias voltage values to be able to attract the electrons through the altered potential
278 field of the spacecraft. Consequently, the electrons could not be measured by the LAP
279 instrument when in sweep mode during about 15 h following impact. The extreme negative
280 spacecraft potential is a clear sign of increased fluxes of electrons to the spacecraft. These
281 increased fluxes of both thermal and suprathermal electrons significantly disturb the LAP
282 measurements for parts of the interval shown in Fig 4. The strongly negative ion current
283 (panel a, negative voltage), which occasionally goes down below -60 nA, and a non-
284 monotonically increasing ion current during individual sweeps, indicates strong dynamics
285 in the plasma and some might be related to secondary electron emissions caused by the
286 impacting energetic electrons. The LAP ion density can therefore not be estimated for
287 large parts of this interval.

288 In Figure 4b, we show the ion and electron densities that still can be estimated, from
289 four independent measurements. LAP provides the ion density from the negative-voltage

290 side of the sweeps (when the spacecraft potential is known) as well as the electron density
291 determined from the spacecraft potential measured by LAP. The ion density might be
292 overestimated when the sweep range only goes down to -18V. As the spacecraft potential
293 is driven significantly negative by the energetic electrons, the electron density derived
294 from the spacecraft potential tends to be overestimated. We therefore chose to be rather
295 conservative and manually lower this estimate by using an electron temperature of 7.5 eV
296 instead of the measured 5 eV in the calculation of the density. MIP provides the electron
297 density when in LDL mode during the long interval on 23 Oct, and the electron density
298 when in SDL mode during the two shorter intervals on 22-23 Oct 2014.

299 Altogether, these four density estimates paint a rather coherent picture (although with
300 some unfortunate data gaps) of how the local plasma density increases by more than an
301 order of magnitude, from $\sim 50 - 300 \text{ cm}^{-3}$ in the interval before impact to $\sim 2000 - 5000$
302 cm^{-3} during the interval when the comet is impacted by the CIR. The MIP density agrees
303 rather well with the available LAP ion density estimates in the high-density interval after
304 impact when the spacecraft potential signal is briefly recovered, as well as before and
305 after impact. However, on 23 Oct the MIP density represents a lower bound since the
306 instrument cut-off at 350 cm^{-3} in LDL mode sets in.

307 The plasma density increases before the identified impact time, already at about 12:00.
308 This is caused by the fact that Rosetta moves toward northern summer latitudes and
309 to over the comet neck region where the neutral outgassing and the plasma density are
310 higher [*Hässig et al.*, 2015; *Edberg et al.*, 2015]. The two short intervals, half and one comet
311 rotation later (6h and 12h), when the density is sufficiently high for MIP to provide a
312 density estimate when in its SDL mode (brown dots), also occur above the neck region.

313 Now the density reaches a maximum of 5000 cm^{-3} . The neutral gas density does not
314 increase by more than a factor of 5 when moving toward the northern latitudes, while the
315 plasma density increases by at least a factor of 10. So the CIR seems to cause the plasma
316 density to at least double during this interval. During the previous and the following orbits
317 when at high latitudes again the plasma density does not increase as much as during the
318 CIR impact event.

319 We also note that both the magnetic field direction (mainly the B_z component) and
320 the energy and flux of suprathermal electrons are observed to vary with a time scale close
321 to half the comet rotation period, indicating that although the solar wind disturbance
322 is large, the interaction region between the cometary plasma environment and the solar
323 wind is still dependent on the structured ionosphere of the comet and its rotation phase.

324 After the CIR impact, the cold plasma density and field strength as well as the energetic
325 ion and electron count rates remain high for about a day before they all go back to more
326 normal values, when the CIR has passed.

327 In Figure 5 we show a zoomed in part from Figure 4 just at the time of impact of the
328 CIR. Here the density data in panel b has been exchanged with the current measurements
329 from LAP1, sampled at a fixed bias potential of +20 V and with a time resolution of
330 35 ms. This current actually anti-correlates with plasma density in this case, as higher
331 density as well as increased flux of suprathermal electrons both serve to drive the S/C
332 potential negative, and this effect overcomes the proportionality of current to density. The
333 drop in current after the CIR impact at 16:30 thus means that the LAP probe no longer
334 sees the electrons, only the ions, as the probe (despite a +20 V bias potential) go negative
335 with respect to the plasma. Nevertheless, the fast variations seen after 17:20 indicate

336 corresponding rapid variations in the plasma, at time scales not possible to resolve in the
337 particle data. An interesting feature occurs at 17:31-17:33 UT, when, simultaneously, the
338 electron current in panel b increases (meaning that the density decreases) for 2 minutes,
339 the magnetic field strength decreases (while still fluctuating as seen in high resolution
340 MAG data - not shown), the energetic electron count decreases significantly, to values
341 lower than before the CIR impact, and the solar wind ion counts decrease significantly.
342 Also the electron current in the LAP sweeps is momentarily retrieved as the S/C potential
343 decreases. These could possibly be the signatures of a plasma boundary forming as the
344 CIR impacts, which Rosetta moves across. We will discuss this possibility further after
345 having presented the remaining three CIR events.

3.3. Event 2: 7 Nov 2014

346 Figure 6 shows a time series of the same format as Figure 4 but covering the interval
347 of the second CIR impact. The second CIR is observed to impact at 14:15 UT on 7 Nov
348 2014 and again causes a significant disturbance to the plasma environment. Rosetta was
349 at this time in orbit at 30 km from the centre of mass, and in the northern illuminated
350 (summer) and more active hemisphere. Both the neutral gas density and the plasma
351 density are naturally lower at this time than when in orbit at 10 km. The CIR impact
352 signatures observed by RPC are similar to those during the previous event: the magnetic
353 field strength and energetic electron fluxes increase suddenly, the LAP ion current changes
354 significantly by about -10 nA, and the spacecraft potential becomes more negative. The
355 cold plasma density more than doubles, from $\sim 50 \text{ cm}^{-3}$ before impact to about ~ 300
356 cm^{-3} immediately after impact, following the sweep-derived electron density. The density
357 estimated from the spacecraft potential probably overestimates the value due to increased

358 fluxes of suprathermal electrons, even though we assume an electron temperature of 10
359 eV during this event. The electron density from the sweep might at the same time be un-
360 derestimated due to the negative spacecraft potential. MIP did not measure any electron
361 plasma oscillations in this interval when it was run in SDL mode, which suggests that the
362 Debye length was much larger than a few tenths of cm. This is consistent with a plasma
363 density that stays below 1000 cm^{-3} for 5-10 eV electrons. Some of the LAP observed
364 density increase is attributed to going toward higher and more illuminated latitudes, but
365 since the latitude continues to increase after the CIR has passed, and the density goes
366 back to nominal values, it is clear that some of the density increase (at least a factor of 2
367 if being conservative) is caused by the CIR impact.

368 The magnetic field strength during this event increases from about 10 nT to 30 nT
369 around the time of impact. The IES suprathermal electron fluxes and ion fluxes increases
370 after impact, similar to the previous event. There are also low-energy ions (10-100 eV)
371 appearing after impact, which might only come into view of the instrument as the magnetic
372 field direction (and consequently the electric field) changes. ICA was on during three short
373 intervals of this event. However, during the passing of the CIR, ICA did measure the solar
374 wind fluxes to be one order of magnitude higher than during the two short intervals prior
375 to and after the CIR impact.

376 There are also significant variations in the magnetic field orientation in this interval,
377 which are simultaneous with the bursts of ~ 100 eV electrons measured by IES (bright
378 yellow patches centered at 16:30, 18:20 and 21:20 UT on 7 Nov 2014 and at 06:00 on 8
379 Nov 2014). The ion current from the LAP probe also increases at these instances. The
380 increased suprathermal electron fluxes during certain magnetic field orientations could

381 indicate that the electrons are heated through the solar wind interaction and accelerated
382 in the direction of the magnetic field. It could also be that the properties of the CIR
383 itself are variable with bursty dynamic pressures enhancements and with a changing IMF
384 direction. The intermittent solar wind signal in IES ion data is partially correlated with
385 the electron and magnetic field signatures as well, which is probably due to the solar wind
386 deflection changing as the IMF changes direction [Broiles *et al.*, 2015].

3.4. Event 3: 3 Dec 2014

387 The third event is shown in Figure 7 in the same format as before. Rosetta was at
388 this time again at a distance of 30 km from the comet nucleus but moving slowly toward
389 southern latitudes. This time the impact of the CIR is much more gradual. There is a
390 less sharp shock front impacting on the comet ionosphere and already on 27 Nov 2014 the
391 solar wind started to increase, as can be seen in the longer overview plot in Figure 2e.
392 However, we will focus on the interval starting on the 3 Dec 2014, when a second pulse of
393 high velocity solar wind reaches the comet. The plasma density increases gradually after
394 the initial impact on 27 Nov, from $\sim 50 \text{ cm}^{-3}$ to values around 200 cm^{-3} . The density
395 estimate from the spacecraft potential may overestimate the values again in this interval
396 even though we have raised the electron temperature in the density estimate model to 10
397 eV. The general density increase occurs when Rosetta is moving toward northern latitudes,
398 where the density should be higher, but on the other hand, the density was about a factor
399 of 2 lower two weeks earlier when previously in the northern hemisphere, meaning that
400 the CIR impact causes a factor of 2 increase in the plasma density. The MIP and LAP
401 density estimates match quite well during this interval.

402 Similar to the previous event, the IES measured fluxes of energetic electrons (yellow
403 bright patches in Figure 7d) appear as very bursty and are correlated with the magnetic
404 field oscillations, and also with the LAP ion current increases (interpreted as a combination
405 of increased density and secondary electron emission).

406 A unique feature of this event is the magnetic field signature. At the same time as the
407 density gradually increases, the magnetic field strength is also gradually increasing, from
408 20 nT at the start of the interval to 50 nT at 18:00 UT on 3 Dec 2014. After this the field
409 strength sharply decreases back to 25 nT. At the same time the solar wind ions disappear
410 from the IES and ICA ion measurements (Figure 7e and g) and are not seen from 18:10
411 - 19:10 UT, likely due to deflection of the solar wind [Broiles *et al.*, 2015]. The ICA solar
412 wind flux measurements (red dots in Figure 7g) provide one data point close to when the
413 magnetic field strength drops to 25 nT, which shows a value two orders of magnitude lower
414 than before, consistent with the solar wind disappearing. The magnetic field strength drop
415 occurs while Rosetta is moving closer to the comet and the distance decreases steadily
416 from 30 km to 25 km over the day (see Figure 2f). After the drop in magnetic field
417 strength there are rapid magnetic field fluctuations, which have not been observed during
418 any of the other events, and the plasma density decreases somewhat. These signatures
419 could be interpreted as the crossing of a plasma boundary, which appears as the solar
420 wind increase compresses the cometary plasma environment. During the 6 hours prior
421 to this major decrease in magnetic field strength, there are four short (~ 10 min) drops
422 in the magnetic field strength, which could then be interpreted as the boundary moving
423 back and forth as the solar wind pressure varies. It could also be that these are signatures

424 of strong dynamics in the plasma environment, a possibility we will expand on further in
425 the Discussion section.

3.5. Event 4: 22 Dec 2014

426 The fourth and final CIR impact also occurs in two steps similar to the previous event,
427 and is shown in Figure 8. The initial impact happened on 22 Dec 2014 at 09:00 UT when
428 Rosetta again was at a distance of 30 km from the comet centre of mass. At impact, the
429 plasma density shows a moderate increase, which is simultaneous with moving towards
430 higher latitudes. The density still increases to a higher value than during the previous
431 pass over the same latitude region, indicating that the CIR again causes the density to
432 increase. The magnetic field strength increases gradually, from about 20 nT to 45 nT,
433 similar to the previous event. The increase lasts until about 20:00 UT on 23 Dec 2014,
434 after which the field strength slowly decreases and the magnetic field orientation slowly
435 changes. On 24 Dec 2015, when the magnetic field orientation has changed, the solar wind
436 flux is decreased and the suprathermal electrons increased significantly. It is possible that
437 these signatures also indicate the crossing of a plasma boundary, which builds up as the
438 solar wind dynamic pressure increases. At 02:00 UT on 25 Dec 2014, the field strength
439 increases briefly and the field changes orientation suddenly.

440 ICA was fortunately on for most of the time during this event and measured increased
441 fluxes of accelerated water ions from the time of impact until noon on 25 Dec 2015, when
442 the CIR had passed (Figure 8f). This also appeared to be the case during CIR event 1,
443 when ICA was on during a few hours around impact. The accelerated water ion fluxes are
444 increased during the entire passing of the CIR and only decreases toward the end of 25
445 Dec 2015. The high fluxes are observed even though the magnetic field changes direction.

446 These accelerated ions are interpreted as the population of pick up ions by the solar wind
447 induced $\mathbf{V} \times \mathbf{B}$ field. As gradient lengths are small compared to the ion gyro-radius,
448 almost all ions will only have seen part of this E-field, giving a broad energy distribution
449 [Nilsson *et al.*, 2015].

450 During the second impact of this event, on 27 Dec 2014, LAP was unfortunately not
451 switched on and MIP was operated in SDL mode, which is blind to 5-10 eV electrons of
452 few hundred particles per cm^{-3} . Still, the signatures in the data from the rest of the RPC
453 instruments (not shown) suggest a similar behaviour as during the other events, except
454 that the magnetic field strength as well as fluxes of energetic electrons are higher in the
455 27 Dec event, and the energetic electrons reach energies of several hundreds of eV.

4. Discussion

456 During the CIR impact events presented here the cold plasma density is seen to increase
457 significantly, but the response is different for each event. During the first event, the
458 cometary ionospheric density is clearly seen to increase, to above 1000 cm^{-3} at 10 km
459 when the CIR impacts, and during the second event the density increases to $\sim 300 \text{ cm}^{-3}$
460 at 30 km. During the third and fourth events, the density increase is more modest but
461 still significant. Hence, each event seems to influence the cometary plasma environment
462 slightly different, in terms of increasing the cold plasma density.

463 The cause of the significant enhancements of the low-energy plasma could be compres-
464 sion of the local plasma by the increased solar wind, particle impact ionisation and/or
465 charge exchange processes when the increased flux of solar wind plasma impacts on the
466 coma. It could also be that more mass-loaded solar wind is accelerated in the direction of
467 the comet ionosphere. The relative increase in the magnetic field strength during event

468 1 is ~ 5 , while the relative increase in the density is $\sim 4-7$. For event 2 the relative in-
469 creases are ~ 4 and ~ 2.5 , respectively. The similar relative increase between the magnetic
470 field strength and the density suggests that compression of the plasma is likely occurring.
471 Furthermore, as the compression leads to an increased density of both the thermal and
472 suprathermal plasma, the ionization rate through particle impact and charge exchange
473 also goes up. An increased ionisation rate gives higher ion pick up rate, which leads to a
474 slowing down of the solar wind. The plasma then gets further compressed as the trailing
475 solar wind catches up, which in turn leads to even more increase in both the density and
476 the magnetic field strength, i.e. the same signatures as seen during direct compression by
477 an increased solar wind dynamic pressure.

478 Comparison between ionospheric models including compression of the plasma and mea-
479 surements of the suprathermal electrons on 23 Oct (during CIR event 1) by Madanian et
480 al., (submitted) show good agreement, which then supports that explanation. ICA does
481 not confirm increased charge exchange (no major increase in He^+ fluxes is observed at
482 this time). The increase in suprathermal electron fluxes ought to cause some increased
483 particle impact ionisation, but to what extent and how much that would increase the
484 density would require further modelling, which is beyond the scope of this paper.

485 The fact that we seem to see a less dramatic increase in the low-energy plasma den-
486 sity during the later events compared to the first event could be because the outgassing
487 increases and the cometary coma becomes more dense when approaching the Sun. A
488 denser coma makes compression harder, and hinders more incoming flux from upstream,
489 such that less solar wind plasma reaches the deep coma where Rosetta was located. As
490 the coma grows, deflection of solar wind plasma also increases due to stronger electric

491 fields [*Broiles et al.*, 2015], resulting in less solar wind plasma reaching the near-nucleus
492 environment [*Nilsson et al.*, 2015]. Also, the solar wind increase is less dramatic during
493 the initial impact in event 4 compared to events 1-3, and we lack LAP data during the
494 main impact.

495 We stress that the density estimates presented here are not without uncertainties and
496 there are several possible sources of errors. These include an uncertain photoelectron
497 current estimate, additional secondary electron emission or a hotter electron temperature
498 and finally, the LAP sweep range being limited and missing parts of the plasma population.
499 Still, using different density estimates from both LAP and MIP, which present rather
500 similar values, provides confidence to the density estimates, and the uncertainty of the
501 relative increase of the density in response to the CIR impact and between the events is
502 nevertheless still quite satisfying.

503 For the first CIR event, a related observation was presented by *Feldman et al.* [2015].
504 They showed measurements from the ALICE far-ultraviolet spectrograph of an increased
505 brightness in the comet limb spectrum on the 22 Oct 2014, i.e. at the time of impact of the
506 first CIR. This was attributed to an increased level of photoelectron impact dissociation
507 of CO₂.

508 During all four CIR impact events, the fluxes of ~ 10 -100 eV electrons are seen to
509 increase significantly. The presence of these electrons, and especially the cause of their
510 energy, is so far unclear [*Clark et al.*, 2015]. They must be accelerated and heated through
511 some mechanism since 100 eV is much higher than what is expected after, for instance,
512 photoionisation (10-15 eV) of neutral species. Here we can report that the acceleration
513 of this population is clearly related to the solar wind interaction since the suprathermal

514 electrons increase in both energy and flux during intervals of increased solar wind energy
515 input. Furthermore, the measured variations in the electron fluxes are apparently con-
516 nected to the magnetic field orientation. These energetic electrons also impact on the
517 spacecraft and drive the spacecraft potential negative, and possibly distort the plasma
518 density measurements by LAP.

519 Another effect that the CIRs might have is that the sputtering of the comet nucleus
520 [*Wurz et al.*, 2015], as well as of larger dust grains, increases as the solar wind particle flux
521 increases. However, this probably does not significantly increase the total plasma density.

522 During event 1, 3, and 4 we observe some unusual signatures in the plasma environment,
523 which are challenging to explain decisively from single spacecraft measurements. In the
524 following paragraphs we will describe these more carefully and discuss if the signatures
525 are either those of plasma boundaries forming in the comet environment, or perhaps
526 the ionospheric response to tail disconnection events. During the first event (Figures 4
527 and 5), about an hour after impact, the magnetic field strength increases, the spacecraft
528 potential becomes less negative so that the measured plasma density decreases and the
529 LAP continuous electron current increases, while the suprathermal electron flux decreases
530 to values lower than before the impact. This could be the signature of skimming a
531 plasma boundary (such as an ionopause or contact surface, for instance), which could
532 be formed briefly at 10 km from the nucleus during a period when the upstream solar
533 wind dynamic pressure is higher than usual. Alternatively, this could be a temporary
534 decrease in the solar wind dynamic pressure, which simply relaxes the disturbance of the
535 cometary plasma environment. However, the fact that both the suprathermal electron
536 fluxes and the magnetic field decreases to values lower than before the impact indicates

537 against this explanation. Also, the LAP sweep during the minute after stands out from all
538 other sweeps during the day, as the spacecraft potential gets less negative than previously,
539 which is consistent with lower density and lower flux of energetic electrons.

540 During event 3 (Figure 7) the magnetic field gradually piles up during several hours
541 after the CIR impact. Then the field strength drops sharply at 18:00 on 3 Dec 2014. Im-
542 mediately after this drop the low-energy plasma density decreases at the same time as a
543 burst of energetic electrons is observed. This could possibly be the signatures of the iono-
544 spheric response of a tail-disconnection event, when magnetic flux is piled-up upstream of
545 the comet before being released during periods of increased solar wind flow. The energetic
546 electrons could have been accelerated into the ionosphere as the piled up magnetic flux
547 is released. A tail-disconnection event could also occur when the diamagnetic cavity is
548 formed, to pre-condition the tail with strong anti-parallel magnetic fields. Although no
549 diamagnetic cavity has been observed in this interval, it is possible that it forms briefly
550 close to the comet following a solar wind pressure pulse.

551 Another possibility is that this is also a plasma boundary forming and as Rosetta
552 moves closer to the comet nucleus and the solar wind increases, the boundary is crossed
553 and Rosetta is entering another plasma region. During event 4, similar signatures are
554 also observed in both the magnetic field and plasma data as the field gradually piles
555 up and a region characterised of high suprathermal fluxes, lower solar wind fluxes and
556 increased fluxes of cometary accelerated water ions is entered. Alternatively, this could
557 again simply be a relaxation of the impinging solar wind dynamic pressure, although
558 then the transition is perhaps sharper than one would expect from a relaxing solar wind.

559 Further work, including modelling and studies of additional events, are required before
560 these observations can be firmly explained.

561 We have shown RPC data from four CIR impacts on comet 67P, during three months in
562 2014, when the comet was relatively inactive. After these, more events have been observed
563 in RPC data on the dates 14 Jan, 29 Jan, 16 Feb, 24 Feb, 6 Mar, 13 Mar, 17 Mar and
564 21 Mar 2015. These events are either CIRs of similar kind as shown in the four examples
565 here or CMEs. In April 2015 the solar wind signal was finally lost in the RPC data since
566 at this time it was being completely shielded/deflected off by the growing cometary coma.
567 Since the cometary activity is constantly increasing the signatures of these events will
568 gradually change and we chose not to study them in any detail here, but rather leave
569 them for a future separate study.

5. Summary

570 CIRs cause a significant disturbance to the cometary plasma environment upon impact.
571 The properties of individual CIRs vary and the response of the cometary plasma environ-
572 ment consequently differs from event to event. We have studied the impact of four CIRs
573 on comet 67P, after having traced them from Earth via Mars and finally to 67P using
574 solar wind monitoring measurements. These solar wind pressure pulses are observed in
575 the interval 22 Oct 2014 to 25 Dec 2014, when the comet was at a heliocentric distance
576 of 3.1 to 2.7 AU. Rosetta was at this time orbiting the comet at a distance of 10-30 km
577 from the nucleus centre of mass. The enhanced solar wind dynamic pressure together
578 with changes in IMF strength and orientation, are the cause of a number of features in
579 the cometary plasma environment out of which the most prominent are outlined below:

580 - the cold (few eV) ionospheric plasma density increases by a factor of at least 2 during
581 three events, due to compression of the plasma environment, increased particle impact
582 ionisation and possibly charge exchange processes, which in turn leads to an increased ion
583 pick up rate.

584 - energetic (10-100 eV) electrons, which appears to be a ubiquitous population around
585 67, are significantly increased in both flux and energy, indicating that these electrons are
586 heated through the solar wind interaction with the cometary plasma. The fluxes vary
587 with changes in the magnetic field direction.

588 - the spacecraft potential drops to values typically below -20 V, as the flux of electrons
589 increase.

590 - accelerated cometary water ions increase in both energy and flux.

591 - the magnetic field piles up around the comet and increases by a factor of 2-5 to reaches
592 values around 50 nT at maximum.

593 - the increased dynamic pressure possibly causes a short-lived (2-3 min) plasma bound-
594 ary to appear on 22 Oct 2014, characterised by a drop in the magnetic field strength,
595 drop-out of energetic electrons and an unusually steady electron current to the LAP
596 probes, followed by an increased electron density the minute after.

597 - on the event on the 3 Nov 2014 the piled up magnetic flux is suddenly released as
598 the magnetic field strength sharply decreases. This is followed by significant magnetic
599 field fluctuations and increased fluxes of energetic electrons over the following 24h. These
600 might be the signatures of a magnetic pile-up boundary having formed or possibly the
601 ionospheric response to a tail disconnection event. Similar features are observed during
602 the fourth CIR event, on 23-25 Dec 2015.

603 In conclusion, the impacting CIRs produce a very dynamic and variable interaction with
604 the rotating comet and its spatially structured and time-varying neutral gas outflow. The
605 magnetic field orientation and strength, energetic electron fluxes, accelerated cometary
606 water ion fluxes and cold plasma density are all varying extensively in the cometary
607 plasma environment. Depending on these properties the CIR interaction with the comet
608 ionosphere will vary accordingly.

609 **Acknowledgments.** Rosetta is a European Space Agency (ESA) mission with contri-
610 butions from its member states and the National Aeronautics and Space Administration
611 (NASA). The work on RPC-LAP data was funded by the Swedish National Space Board
612 under contracts 109/02, 135/13, 166/14 and 114/13 and Vetenskapsrådet under contracts
613 621-2013-4191 and 621-2014-5526. This work has made use of the AMDA and RPC Quick-
614 look database to provide an initial overview of the events studied. This is provided through
615 a collaboration between the Centre de Données de la Physique des Plasmas (CDPP) (sup-
616 ported by CNRS, CNES, Observatoire de Paris and Université Paul Sabatier, Toulouse)
617 and Imperial College London (supported by the UK Science and Technology Facilities
618 Council). We thank K.C. Hansen and B. Zieger for providing solar wind propagations
619 from their Michigan Solar Wind Model (<http://mswim.engin.umich.edu/>). The data used
620 in this paper will soon be made available on the ESA Planetary Science Archive and is
621 available upon request until that time.

References

622 Barabash, S., R. Lundin, H. Andersson, K. Brinkfeldt, A. Grigoriev, H. Gunell, M. Holm-
623 ström, M. Yamauchi, K. Asamura, P. Bochsler, P. Wurz, R. Cerulli-Irelli, A. Mura,

624 A. Milillo, M. Maggi, S. Orsini, A. J. Coates, D. R. Linder, D. O. Kataria, C. C. Curtis,
625 K. C. Hsieh, B. R. Sandel, R. A. Frahm, J. R. Sharber, J. D. Winningham, M. Grande,
626 E. Kallio, H. Koskinen, P. Riihelä, W. Schmidt, T. Säles, J. U. Kozyra, N. Krupp,
627 J. Woch, S. Livi, J. G. Luhmann, S. McKenna-Lawlor, E. C. Roelof, D. J. Williams,
628 J.-A. Sauvaud, A. Fedorov, and J.-J. Thocaven (2006), The Analyzer of Space Plasmas
629 and Energetic Atoms (ASPERA-3) for the Mars Express mission, *Space Sci. Rev.*, *126*,
630 113–164, doi:10.1007/s11214-006-9124-8.

631 Broiles, T., J. Burch, Clark, G.B., Koenders, C., Behar, E., Goldstein, R., Fuselier, S.A.,
632 Mandt, K.E., Mokashi, P., and Samara, M. (2015), Rosetta observations of solar wind in-
633 teraction with the comet 67p/churyumov-gerasimenko, "*Astronomy and Astrophysics*",
634 doi:10.1051/0004-6361/201526046.

635 Burch, J. L., R. Goldstein, T. E. Cravens, W. C. Gibson, R. N. Lundin, C. J. Pollock,
636 J. D. Winningham, and D. T. Young (2007), RPC-IES: The Ion and Electron Sensor
637 of the Rosetta Plasma Consortium, *Space Sci. Rev.*, *128*, 697–712, doi:10.1007/s11214-
638 006-9002-4.

639 Burch, J. L., T. E. Cravens, K. Llera, R. Goldstein, P. Mokashi, C.-Y. Tzou, and
640 T. Broiles (2015), Charge exchange in cometary coma: Discovery of h^+ ions in the
641 solar wind close to comet 67p/churyumov-gerasimenko, *Geophysical Research Letters*,
642 doi:10.1002/2015GL064504, 2015GL064504.

643 Carr, C., E. Cupido, C. G. Y. Lee, A. Balogh, T. Beek, J. L. Burch, C. N. Dunford, A. I.
644 Eriksson, R. Gill, K. H. Glassmeier, R. Goldstein, D. Lagoutte, R. Lundin, K. Lundin,
645 B. Lybekk, J. L. Michau, G. Musmann, H. Nilsson, C. Pollock, I. Richter, and J. G.
646 Trotignon (2007), RPC: The Rosetta Plasma Consortium, *Space Sci. Rev.*, *128*, 629–

647 647, doi:10.1007/s11214-006-9136-4.

648 Clark, G., Broiles, T. W., Burch, J. L., Collinson, G. A., Cravens, T., Frahm, R. A.,
649 Goldstein, J., Goldstein, R., Mandt, K., Mokashi, P., Samara, M., and Pollock, C.
650 J. (2015), Suprathermal electron environment of comet 67p/churyumov-gerasimenko:
651 Observations from the rosetta ion and electron sensor, *Astronomy and Astrophysics*,
652 doi:10.1051/0004-6361/201526351.

653 Cravens, T. E., J. U. Kozyra, A. F. Nagy, T. I. Gombosi, and M. Kurtz (1987), Electron
654 impact ionization in the vicinity of comets, *Journal of Geophysical Research: Space*
655 *Physics*, *92*(A7), 7341–7353, doi:10.1029/JA092iA07p07341.

656 Dubinin, E., R. Modolo, M. Fränz, J. Woch, F. Akalin, D. Gurnett, R. Lundin,
657 S. Barabash, J. J. Plaut, and G. Picardi (2008), Structure and dynamics of the solar
658 wind/ionosphere interface on Mars. MEX-ASPERA-3 and MEX-MARSIS observations,
659 *Geophys. Res. Lett.*, *35*, L11,103, doi:10.1029/2008GL033730.

660 Edberg, N. J. T., U. Auster, S. Barabash, A. Bößwetter, D. A. Brain, C. M. Carr, S. W. H.
661 Cowley, E. Cupido, F. Duru, A. I. Eriksson, M. Fränz, K.-H. Glassmeier, R. Goldstein,
662 M. Lester, R. Lundin, R. Modolo, H. Nilsson, I. Richter, M. Samara, and J. G. Trotignon
663 (2009), Rosetta and Mars Express observations of the influence of high solar wind
664 dynamic pressure on the Martian plasma environment, *Ann. Geophys.*, *27*, 4533–4545,
665 doi:10.5194/angeo-27-4533-2009.

666 Edberg, N. J. T., H. Nilsson, A. O. Williams, M. Lester, S. E. Milan, S. W. H. Cow-
667 ley, M. Fränz, S. Barabash, and Y. Futaana (2010), Pumping out the atmosphere
668 of Mars through solar wind pressure pulses, *Geophys. Res. Lett.*, *37*, L03,107, doi:
669 10.1029/2009GL041814.

- 670 Edberg, N. J. T., H. Nilsson, Y. Futaana, G. Stenberg, M. Lester, S. W. H. Cowley, J. Luh-
671 mann, T. R. McEnulty, A. Fedorov, S. Barabash, and T. L. Zhang (2011), Atmospheric
672 erosion of Venus during stormy space weather, *Geophys. Res. Lett.* (*submitted*).
- 673 Edberg, N. J. T., A. I. Eriksson, E. Odelstad, P. Henri, J.-P. Lebreton, S. Gasc, M. Rubin,
674 M. Andr, R. Gill, E. P. G. Johansson, F. Johansson, E. Vigren, J. E. Wahlund, C. M.
675 Carr, E. Cupido, K.-H. Glassmeier, R. Goldstein, C. Koenders, K. Mandt, Z. Nemeth,
676 H. Nilsson, I. Richter, G. S. Wieser, K. Szego, and M. Volwerk (2015), Spatial distribu-
677 tion of low-energy plasma around comet 67p/cg from rosetta measurements, *Geophysical*
678 *Research Letters*, *42*, doi:10.1002/2015GL064233, 2015GL064233.
- 679 Eriksson, A. I., R. Boström, R. Gill, L. Åhlén, S.-E. Jansson, J.-E. Wahlund, M. André,
680 A. Mälkki, J. A. Holtet, B. Lybekk, A. Pedersen, and L. G. Blomberg (2007), RPC-
681 LAP: The Rosetta Langmuir Probe Instrument, *Space Sci. Rev.*, *128*, 729–744, doi:
682 10.1007/s11214-006-9003-3.
- 683 Feldman, P., M. F. A’Hearn, J.-L. Bertaux, L. M. Feaga, J. W. Parker, E. Schindhelm,
684 A. J. Steffl, S. A. Stern, H. A. Weaver, H. Sierks, and J.-B. Vincent (2015), Measure-
685 ments of the near-nucleus coma of comet 67p churyumov-gerasimenko with the alice far-
686 ultraviolet spectrograph on rosetta, *”Astronomy and Astrophysics”*, doi:”10.1051/0004-
687 6361/201525925”.
- 688 Glassmeier, K.-H., I. Richter, A. Diedrich, G. Musmann, U. Auster, U. Motschmann,
689 A. Balogh, C. Carr, E. Cupido, A. Coates, M. Rother, K. Schwingenschuh, K. Szegö,
690 and B. Tsurutani (2007), RPC-MAG The Fluxgate Magnetometer in the ROSETTA
691 Plasma Consortium, *Space Sci. Rev.*, *128*, 649–670, doi:10.1007/s11214-006-9114-x.

- 692 Goldstein, R., J. L. Burch, P. Mokashi, T. Broiles, K. Mandt, J. Hanley, T. Cravens,
693 A. Rahmati, M. Samara, G. Clark, M. Hässig, and J. M. Webster (2015), The
694 rosetta ion and electron sensor (ies) measurement of the development of pickup
695 ions from comet 67p/churyumov-gerasimenko, *Geophys. Res. Lett.*, pp. n/a–n/a, doi:
696 10.1002/2015GL063939.
- 697 Gulkis, S., M. Allen, P. von Allmen, G. Beaudin, N. Biver, D. Bockele-Morvan,
698 M. Choukroun, J. Crovisier, B. J. R. Davidsson, P. Encrenaz, T. Encrenaz, M. Frerk-
699 ing, P. Hartogh, M. Hofstadter, W.-H. Ip, M. Janssen, C. Jarchow, S. Keihm, S. Lee,
700 E. Lellouch, C. Leyrat, L. Rezac, F. P. Schloerb, and T. Spilker (2015), Subsurface
701 properties and early activity of comet 67p/churyumov-gerasimenko, *Science*, *347*(6220),
702 doi:10.1126/science.aaa0709.
- 703 Halekas, J., E. Taylor, G. Dalton, G. Johnson, D. Curtis, J. McFadden, D. Mitchell,
704 R. Lin, and B. Jakosky (2013), The solar wind ion analyzer for maven, *Space Sci. Rev.*,
705 pp. 1–27, doi:10.1007/s11214-013-0029-z.
- 706 Hässig, M., K. Altwegg, H. Balsiger, A. Bar-Nun, J. J. Berthelier, A. Bieler, P. Bochsler,
707 C. Briois, U. Calmonte, M. Combi, J. De Keyser, P. Eberhardt, B. Fiethe, S. A. Fuselier,
708 M. Galand, S. Gasc, T. I. Gombosi, K. C. Hansen, A. Jckel, H. U. Keller, E. Kopp,
709 A. Korth, E. Khrt, L. Le Roy, U. Mall, B. Marty, O. Mousis, E. Neefs, T. Owen,
710 H. Rme, M. Rubin, T. Smon, C. Tornow, C.-Y. Tzou, J. H. Waite, and P. Wurz (2015),
711 Time variability and heterogeneity in the coma of 67p/churyumov-gerasimenko, *Science*,
712 *347*(6220), doi:10.1126/science.aaa0276.
- 713 Koenders, C., K.-H. Glassmeier, I. Richter, U. Motschmann, and M. Rubin (2013),
714 Revisiting cometary bow shock positions, *Planet. Space Sci.*, *87*(0), 85 – 95, doi:

- 715 <http://dx.doi.org/10.1016/j.pss.2013.08.009>.
- 716 Niedner, M. B., Jr., and J. C. Brandt (1978), Interplanetary gas. XXII - Plasma tail
717 disconnection events in comets - Evidence for magnetic field line reconnection at inter-
718 planetary sector boundaries, *Astrophys. J.*, *223*, 655–670, doi:10.1086/156299.
- 719 Nilsson, H., R. Lundin, K. Lundin, S. Barabash, H. Borg, O. Norberg, A. Fedorov, J.-A.
720 Sauvaud, H. Koskinen, E. Kallio, P. Riihelä, and J. L. Burch (2007), RPC-ICA: The
721 Ion Composition Analyzer of the Rosetta Plasma Consortium, *Space Sci. Rev.*, *128*,
722 671–695, doi:10.1007/s11214-006-9031-z.
- 723 Nilsson, H., G. Stenberg Wieser, E. Behar, C. S. Wedlund, H. Gunell, M. Yamauchi,
724 R. Lundin, S. Barabash, M. Wieser, C. Carr, E. Cupido, J. L. Burch, A. Fedorov, J.-A.
725 Sauvaud, H. Koskinen, E. Kallio, J.-P. Lebreton, A. Eriksson, N. Edberg, R. Goldstein,
726 P. Henri, C. Koenders, P. Mokashi, Z. Nemeth, I. Richter, K. Szego, M. Volwerk,
727 C. Vallat, and M. Rubin (2015), Birth of a comet magnetosphere: A spring of water
728 ions, *Science*, *347*(6220), doi:10.1126/science.aaa0571.
- 729 Nilsson, H., Stenberg Wieser, G., Behar, E., Simon Wedlund, C., Kallio, E., Edberg, N.,
730 Eriksson, A. I., Yamauchi, M., Koenders, C., Wieser, M., Lundin, R., Barabash, S.,
731 Mandt, K., Burch, J. L., Goldstein, R., Mokashi, P., Carr, C., Cupido, E., Fox, P. T.,
732 and ... (2015), Evolution of the ion environment of comet 67p/churyumov-gerasimenko
733 - observations between 3.6 and 2.0 au, *Astronomy and Astrophysics*, doi:10.1051/0004-
734 6361/201526142.
- 735 Odelstad, E., A. I. Eriksson, N. J. T. Edberg, F. Johansson, E. Vigren, M. Andr, C.-Y.
736 Tzou, C. Carr, and E. Cupido (2015), Evolution of the plasma environment of comet
737 67p from spacecraft potential measurements by the rosetta langmuir probe instrument,

- 738 *Geophys. Res. Lett.*, *42*(23), 10,126–10,134, doi:10.1002/2015GL066599, 2015GL066599.
- 739 Ramstad, R., S. Barabash, Y. Futaana, H. Nilsson, X.-D. Wang, and M. Holmström (2015),
740 The martian atmospheric ion escape rate dependence on solar wind and solar euV con-
741 ditions i: Seven years of Mars Express observations, *Journal of Geophysical Research:*
742 *Planets*, pp. n/a–n/a, doi:10.1002/2015JE004816, 2015JE004816.
- 743 Richter, I., C. Koenders, H.-U. Auster, D. Frühauff, C. Götzt, P. Heinisch, C. Perschke,
744 U. Motschmann, B. Stoll, K. Altwegg, J. Burch, C. Carr, E. Cupido, A. Eriksson,
745 P. Henri, R. Goldstein, J.-P. Lebreton, P. Mokashi, Z. Nemeth, H. Nilsson, M. Rubin,
746 K. Szegö, B. T. Tsurutani, C. Vallat, M. Volwerk, and K.-H. Glassmeier (2015), Ob-
747 servation of a new type of low-frequency waves at comet 67P/Churyumov-Gerasimenko,
748 *Ann. Geophys.*, *33*(8), 1031–1036, doi:10.5194/angeo-33-1031-2015.
- 749 Rubin, M., C. Koenders, K. Altwegg, M. Combi, K.-H. Glassmeier, T. Gombosi,
750 K. Hansen, U. Motschmann, I. Richter, V. Tenishev, and G. Toth
751 (2014), Plasma environment of a weak comet: Predictions for comet
752 67P/Churyumov-Gerasimenko from multifluid-MHD and hybrid models, *Icarus*, *242*,
753 38 – 49, doi:http://dx.doi.org/10.1016/j.icarus.2014.07.021.
- 754 Trotignon, J. G., J. L. Michau, D. Lagoutte, M. Chabassière, G. Chalumeau, F. Colin,
755 P. M. E. Décreau, J. Geiswiler, P. Gille, R. Grard, T. Hachemi, M. Hamelin, A. Eriksson,
756 H. Laakso, J. P. Lebreton, C. Mazelle, O. Randriamboarison, W. Schmidt, A. Smit,
757 U. Telljohann, and P. Zamora (2007), RPC-MIP: the Mutual Impedance Probe of the
758 Rosetta Plasma Consortium, *Space Sci. Rev.*, *128*, 713–728, doi:10.1007/s11214-006-
759 9005-1.

- 760 Vigren, E., M. Galand, A. I. Eriksson, N. J. T. Edberg, E. Odelstad, and S. Schwartz
761 (2015), On the electron to neutral number density ratio in the coma of comet
762 67P/Churyumov-Gerasimenko: guiding expression and sources for deviations, *Astro-*
763 *phys. J., in press.*
- 764 Volwerk, M., I. Richter, B. Tsurutani, C. Gtz, K. Altwegg, T. Broiles, J. Burch, C. Carr,
765 E. Cupido, M. Delva, M. Dsa, N. J. T. Edberg, A. Eriksson, P. Henri, C. Koenders,
766 J.-P. Lebreton, K. E. Mandt, H. Nilsson, A. Opitz, M. Rubin, K. Schwingenschuh,
767 G. Stenberg Wieser, K. Szeg, C. Vallat, X. Vallieres, and K.-H. Glassmeier (2016),
768 Mass-loading, pile-up, and mirror-mode waves at comet 67p/churyumov-gerasimenko,
769 *Ann. Geophys.*, *34*(1), 1–15, doi:10.5194/angeo-34-1-2016.
- 770 Vourlidas, A., C. J. Davis, C. J. Eyles, S. R. Crothers, R. A. Harrison, R. A. Howard, J. D.
771 Moses, and D. G. Socker (2007), First direct observation of the interaction between a
772 comet and a coronal mass ejection leading to a complete plasma tail disconnection, *The*
773 *Astrophysical Journal Letters*, *668*(1), L79.
- 774 Wurz, P., Rubin, M., Altwegg, K., Balsiger, H., Gasc, S., Galli, A., Jäckel, A., Le Roy,
775 L., Calmonte, U., Tzou, C., Mall, U.A., Fiethe, B., De Keyser, J., Berthelier, J.J.,
776 Reme, H., Bieler, A., Tenishev, V., Gombosi, T.I., and Fuselier, S.A. (2015), "solar
777 wind sputtering of dust on the surface of 67p/churyumov-gerasimenko", *Astronomy*
778 *and Astrophysics*, doi:10.1051/0004-6361/201525980.
- 779 Zieger, B., and K. C. Hansen (2008), Statistical validation of a solar wind propagation
780 model from 1 to 10 au, *Journal of Geophysical Research: Space Physics*, *113*(A8), n/a–
781 n/a, doi:10.1029/2008JA013046, a08107.

Figure 1. Positions of Earth, Mars and comet 67P during three months in late 2014 in ecliptic J2000 coordinates. In this interval the passings of 4 CIRs were observed from solar wind measurements at each celestial body. The times of impacts are indicated by filled circles.

Figure 2. Time series of (a and b) solar wind density and speed from ACE at Earth, (c and d) solar wind speed and density from Mars Express (black) and MAVEN (blue) at Mars, (e) Rosetta/IES ion spectrogram (summed over all azimuths and sectors), together with the solar wind velocity from the mSWIM model (magenta) and (f) distance between Rosetta and the comet centre of mass. The red vertical bars indicate the impact time of the CIRs, as determined from the Rosetta data.

Figure 3. The position of Rosetta in the comet-centred CSO reference frame during the four CIR impacts. The sun is toward positive X_{CSO} . The positions are shown for the same intervals as the time series in Figures 4-8. The events are numbered at the beginning of the interval and the position at impact is indicated by the red circle. Impact of event three occurred before the time series started. The projections of the position on the x-y, x-z and y-z planes are shown in grey.

Figure 4. Times series of combined RPC data from the time around the first CIR impact. The panels show (a) LAP bias voltage sweeps (depending on telemetry available the sweep range varies), (b) plasma density estimates from LAP and MIP, (c) vector magnetic field and magnitude from MAG, (d) electron spectrogram from IES, (e) ion spectrogram, (f) spectrogram of cometary water ions from ICA, (g) spectrogram of solar wind ions from ICA together with solar wind flux (red dots) and finally, (h) cometary longitude (blue line) and latitude (black) of Rosetta. All spectrograms are summed over all elevation and azimuth sectors. The time of impact is indicated by the red vertical line. Note the significant increase in plasma density, magnetic field strength, energetic electron flux and water ion flux at impact.

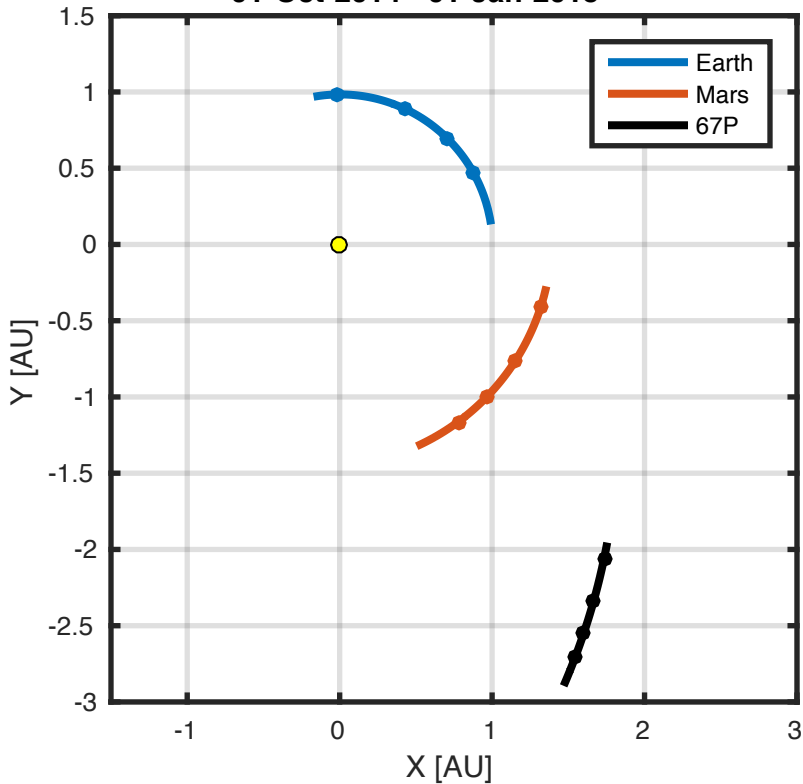
Figure 5. Zoom in from Figure 4 during one hour around impact of the first CIR. The format is the same except for that in panel 2 we now show the high-resolution fixed-bias current sampled by LAP1 rather than the density. The bias voltage is +20 V.

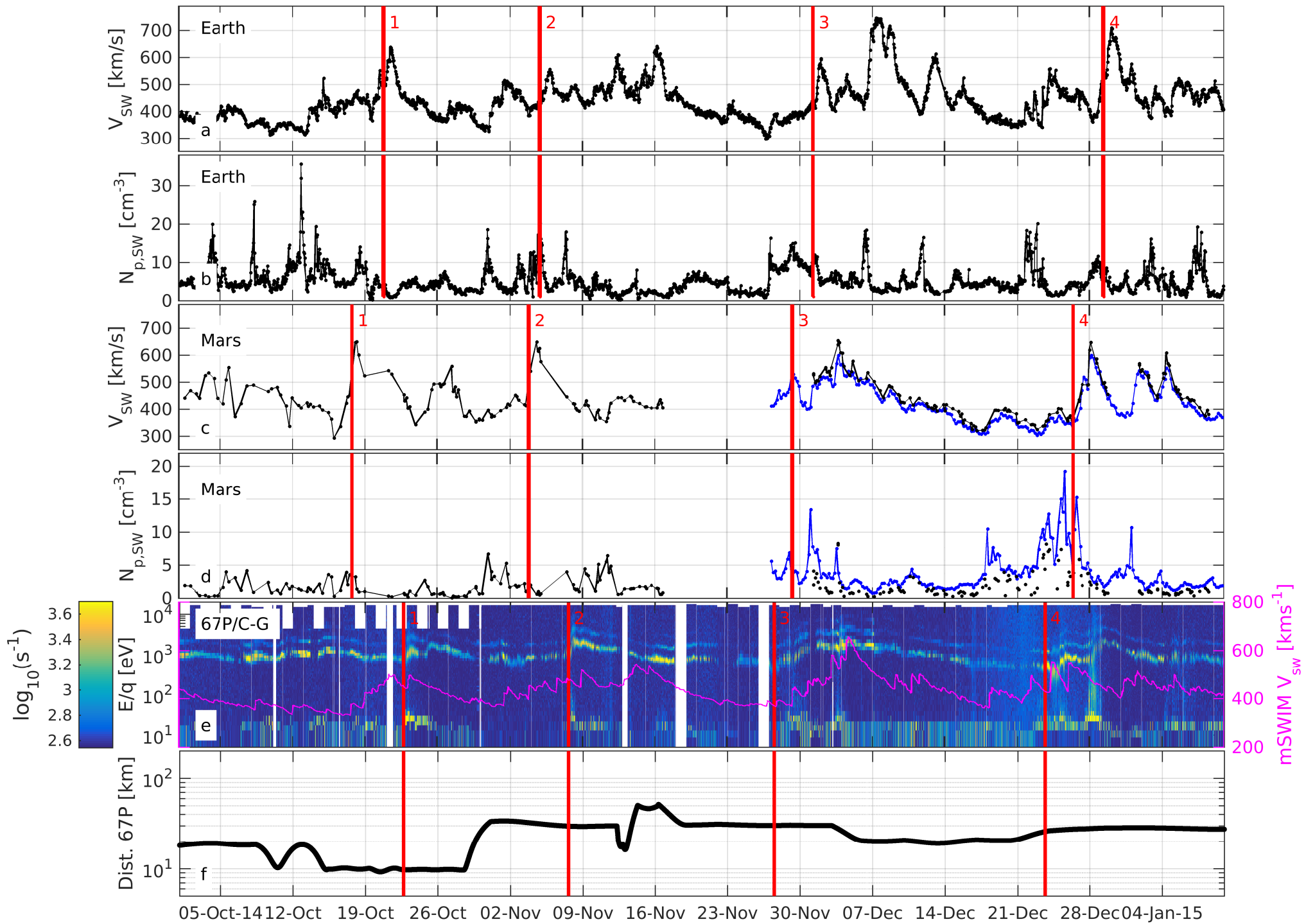
Figure 6. Same as Figure 4 but for the second CIR impact. Note again the significant increase in plasma density, magnetic field strength and energetic electrons after impact. The large scale oscillations (time scale of hours) in magnetic field correlates with LAP sweep variations and an increase in the energetic (~ 100 eV) electrons from IES.

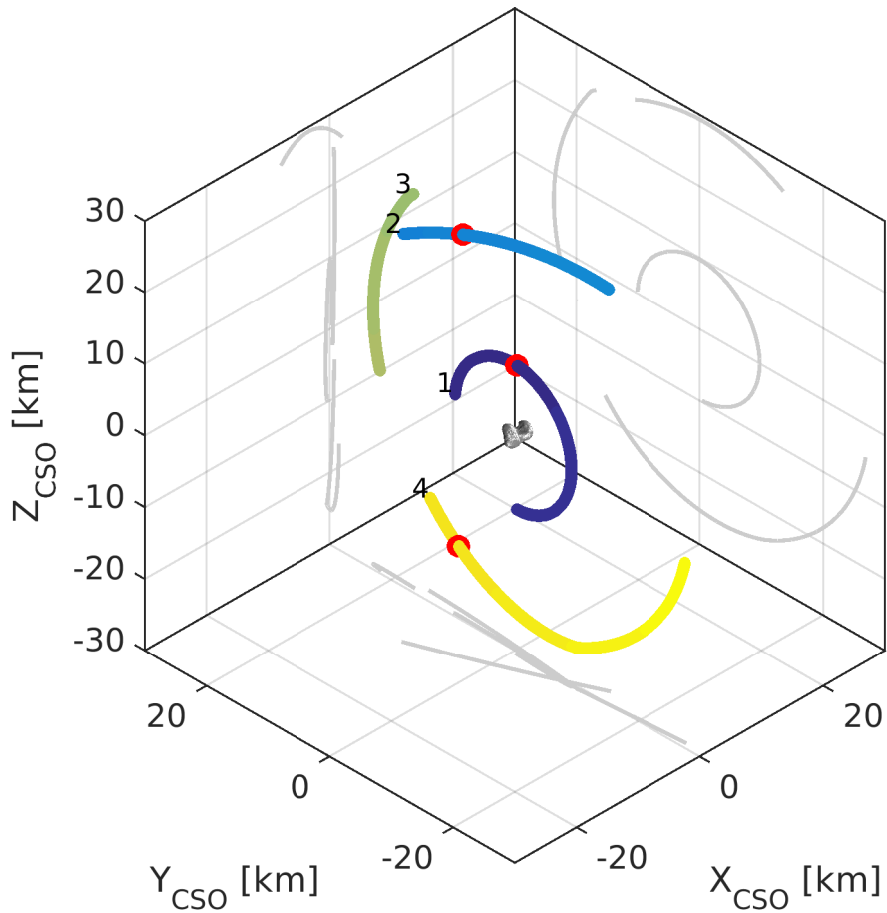
Figure 7. Same as Figure 4 but for the third CIR event. The initial CIR impact occurs already on 27 Nov 2014, but continues over several days and covers the interval shown here. In the interval shown here (still during the passing of the CIR) there is a gradual increase in both plasma density and magnetic field strength, which is followed by a sudden drop in magnetic field strength and an increase in magnetic field fluctuations over the following 24 h. At the same time the 100 eV electron flux is further increased compared to quiet solar wind times.

Figure 8. Same as Figure 4 but for the fourth CIR impact. Note the large scale change in the magnetic field orientation and the modest increase in plasma density. There is an increase in density immediately after the CIR impact, particularly seen as that is when MIP starts observing features at the plasma frequency in the mutual impedance spectra to provide density estimates. This is consistent with a discontinuity toward a smaller Debye length at the CIR impact. The energetic electrons still appear in this interval but are most prominent 1.5 days after impact, at the same time as the solar wind flux decreases. Water ion fluxes of energies up to 100 eV are elevated during the entire interval.

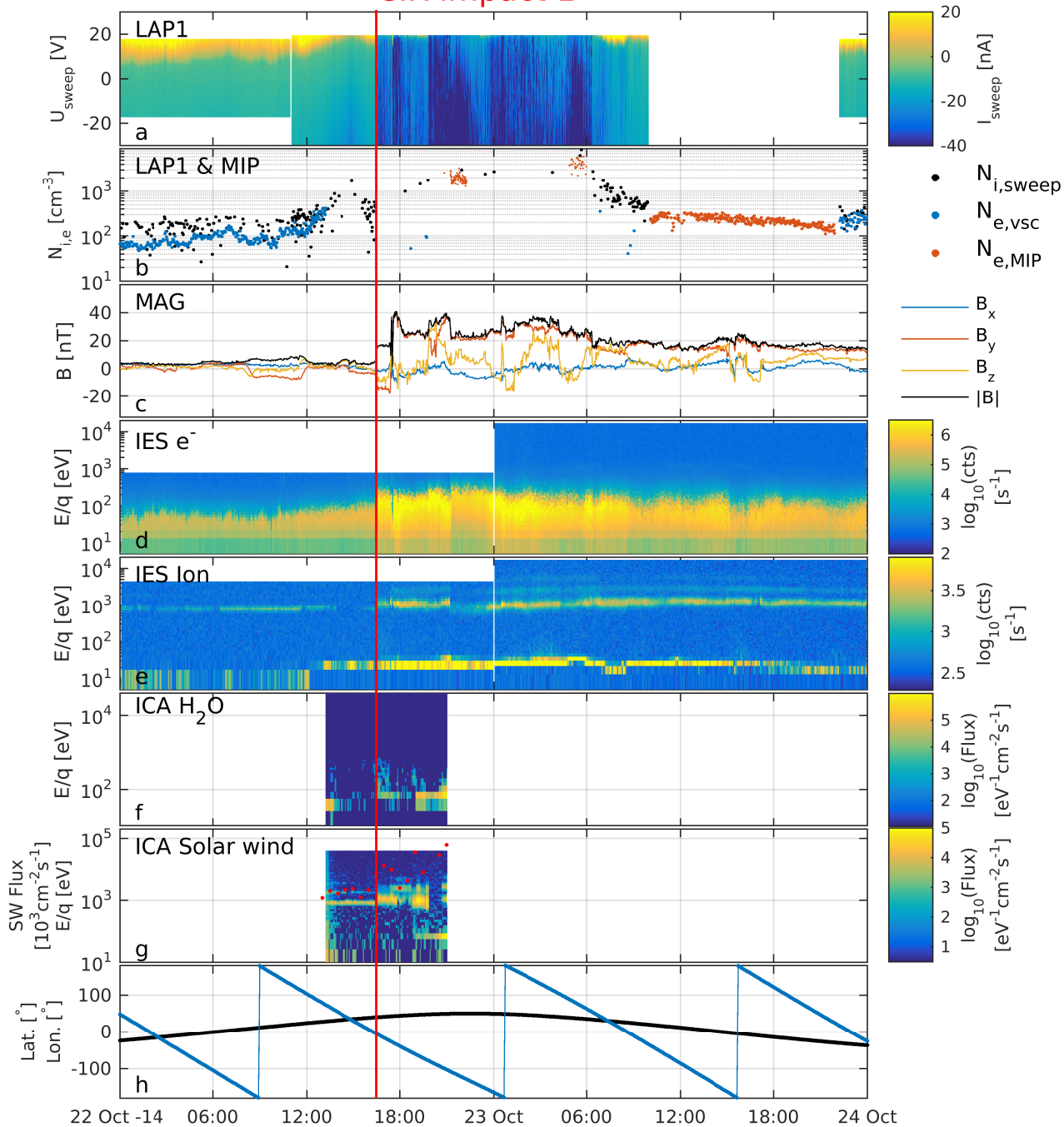
01-Oct-2014 - 01-Jan-2015





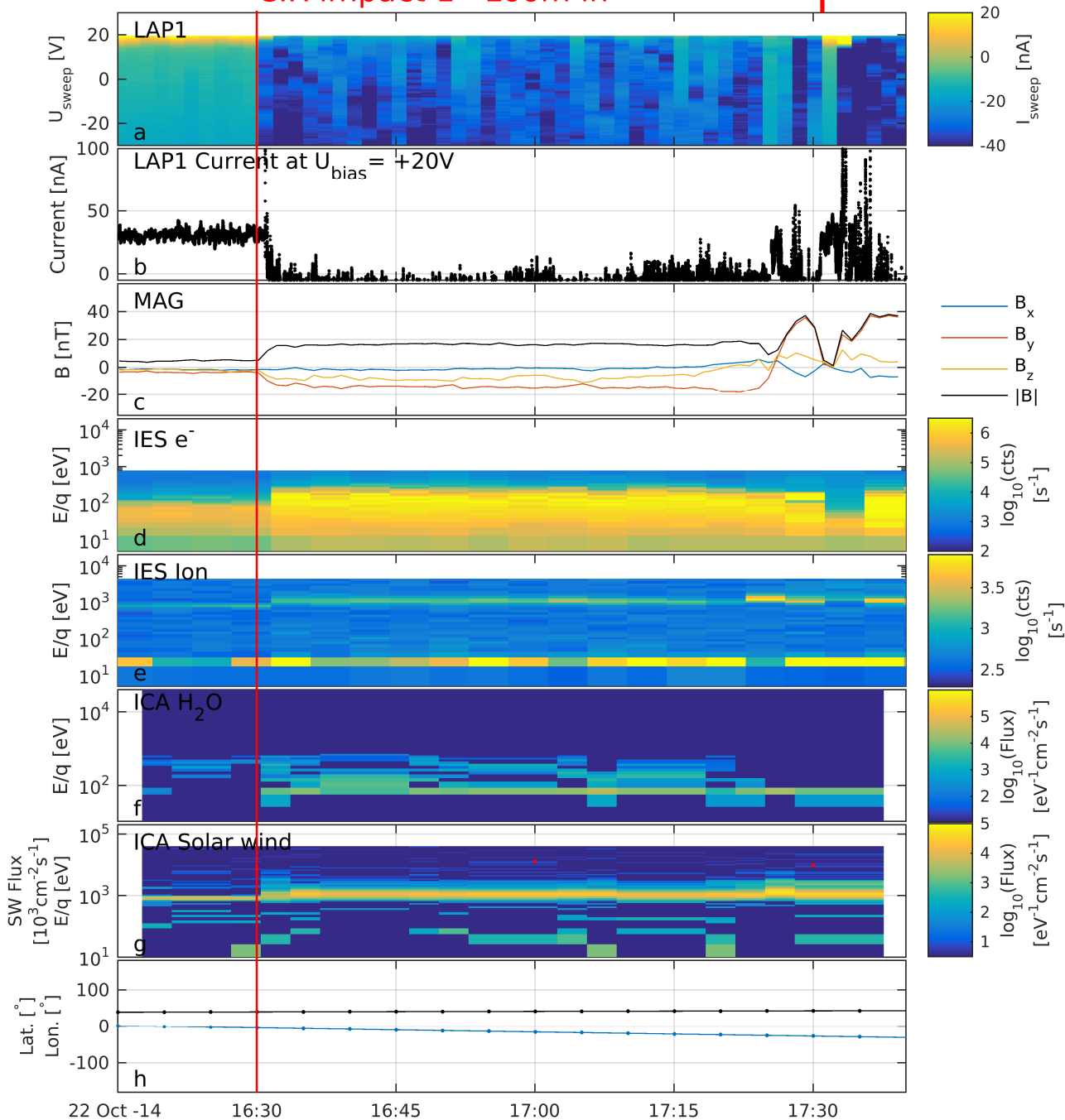


CIR impact 1

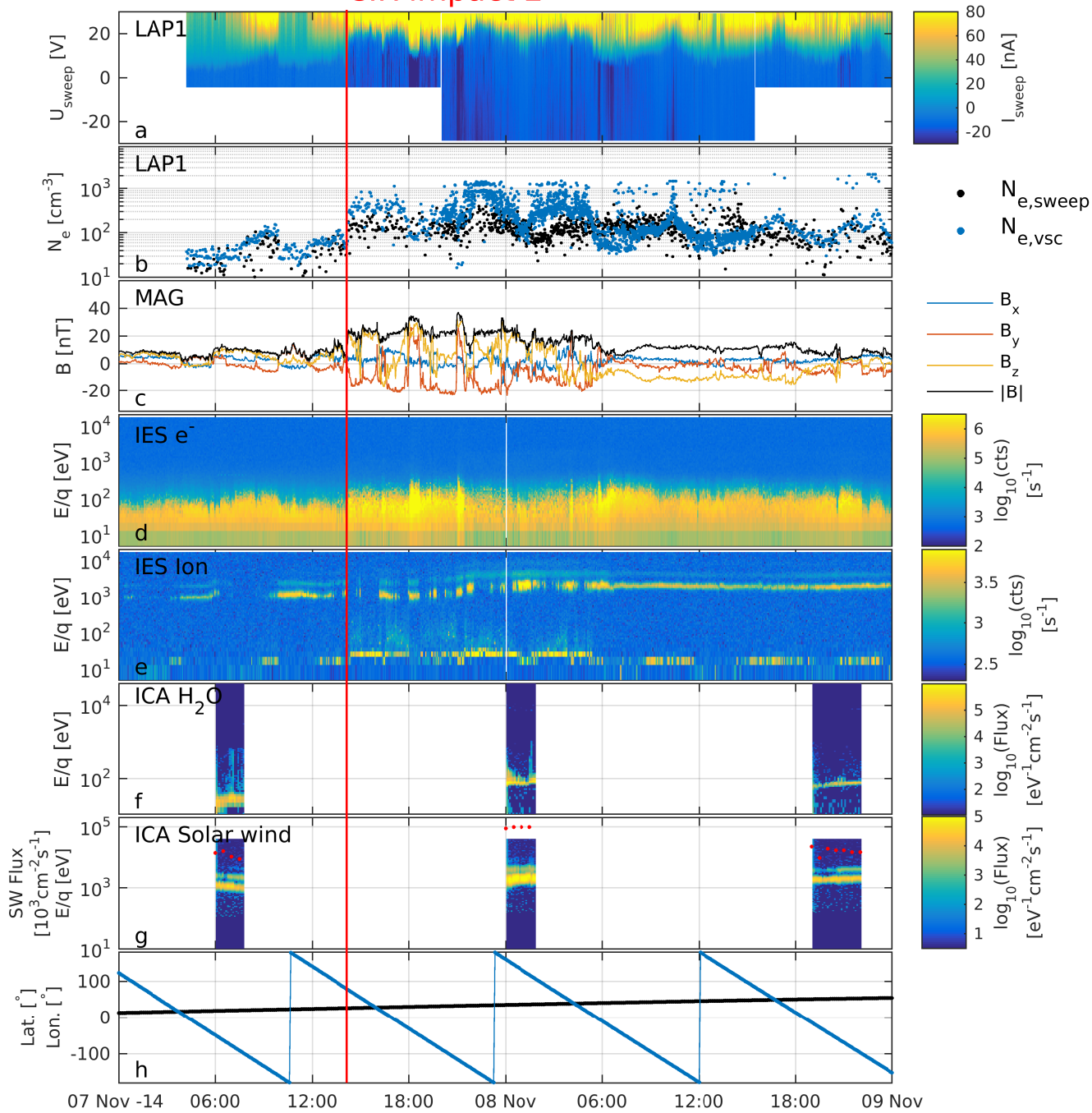


CIR impact 1 - zoom in

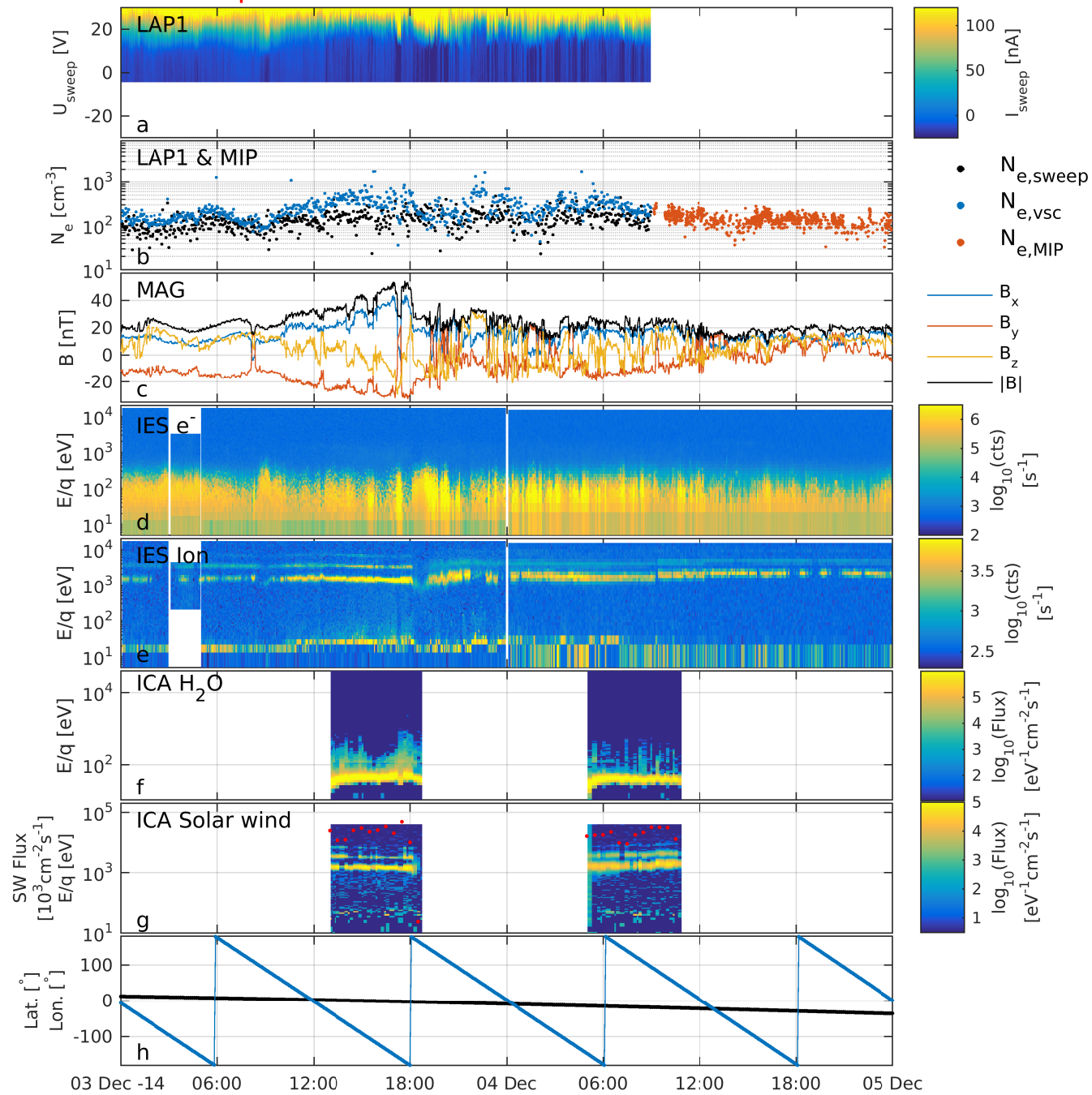
Boundary crossing?



CIR impact 2



← CIR impact 3



CIR impact 4

